

Generation of Ultrahigh-Velocity Ionizing Shocks with Petawatt-Class Laser Pulses

P. M. Nilson,^{1,*} S. P. D. Mangles,¹ L. Willingale,^{1,†} M. C. Kaluza,^{1,‡} A. G. R. Thomas,^{1,†} M. Tatarakis,² Z. Najmudin,¹ R. J. Clarke,³ K. L. Lancaster,² S. Karsch,⁴ J. Schreiber,^{4,5} R. G. Evans,¹ A. E. Dangor,¹ and K. Krushelnick^{1,†}

¹*Department of Physics, Imperial College, London SW7 2AZ United Kingdom*

²*Technological Educational Institute of Crete, Romanou, 3-GR73133 Chania, Greece*

³*CLF, Rutherford Appleton Laboratory, Chilton, Didcot, Oxon., OX11 0QX United Kingdom*

⁴*Max-Planck Institut für Quantenoptik, Hans-Kopfermann-Straße, D-85748, Garching, Germany*

⁵*Ludwig-Maximilians-Universität München, Am Coulombwall, D-85748, Garching, Germany*

(Received 1 October 2009; published 16 December 2009)

Ultrahigh-velocity shock waves ($\sim 10\,000$ km/s or $0.03c$) are generated by focusing a 350-TW laser pulse into low-density helium gas. The collisionless ultrahigh-Mach-number electrostatic shock propagates from the plasma into the surrounding gas, ionizing gas as it becomes collisional. The shock undergoes a corrugation instability due to propagation of the ionizing shock within the gas (the Dyakov-Kontorovich instability). This system may be relevant to the study of very high-Mach-number ionizing shocks in astrophysical situations.

DOI: 10.1103/PhysRevLett.103.255001

PACS numbers: 52.35.Tc, 52.50.Jm, 52.72.+v

The passage of strong and/or relativistic shock waves and the effects of radiation processes [1,2] determine much of the observed structure in the interstellar medium. Many aspects of these complex interactions are not well understood—from the energy-dissipation mechanisms associated with the collisionless limit, to the stability of both radiative and nonradiative collisional shock waves. There is much interest, therefore, in producing very high-Mach-number shock waves in the laboratory to study the evolution of their properties and to measure the characteristics of any resulting instabilities.

Previous laboratory studies of laser-driven blast waves have investigated the evolution of front formation by varying the target composition, laser energy, pulse duration, and focused intensity [3–5] as well as the effect of radiation. A less-studied problem concerns collisionless electrostatic shocks [6], their associated dissipation mechanisms, and the subsequent relaxation into the collision-dominated regime, along with the effect of ionization processes. Such shocks are common in plasmas associated with supernova remnants and can be created following a dramatic release of energy. No single analytical theory describes such high-Mach-number, ionizing nonradiative shocks, yet they are important for a large number of astrophysical situations. For example, the structure observed in the emission of neutral hydrogen in SN 1006 and the Northern Cygnus Loop has been attributed to such instabilities [7].

This Letter describes the results of an experiment that investigated electrostatic shock formation in a low-density, nonradiative (helium) plasma with an ultrahigh-intensity laser-plasma interaction. We show for the first time the development of ultrahigh-Mach-number ionizing shocks and their associated instabilities. The use of a new generation of “petawatt-class” laser systems in such experiments makes it possible to generate shock waves having velocities that are orders of magnitude higher than those pro-

duced by any other laboratory method. The observed velocities in our experiments begin to approach the relativistic regime, and with laser systems presently planned for construction in the near future [8], it will soon be possible to study relativistic shock waves in the laboratory for the first time. The conditions created here present a novel laser-driven blast wave study at intensities greater than any previously reported ($>10^{20}$ W/cm²) with a much-higher Mach number and in a more astrophysically relevant, low- Z plasma, where radiation effects can be largely ignored.

The experiment was carried out on the Vulcan Petawatt laser facility at the Rutherford Appleton Laboratory in the UK. The laser delivered 1-ps-duration pulses with energies of 200 to 350 J at a wavelength of $1.054\ \mu\text{m}$. A 180-cm-focal-length, $f/3$ off-axis parabolic mirror was used to focus the beam to a vacuum focal spot of 6 to $7\ \mu\text{m}$, full width at half maximum, giving a peak vacuum intensity of $4 \pm 1 \times 10^{20}$ W/cm². Such parameters define a normalized amplitude for the vector potential of $a_0 = eE/m_e c \omega_0 > 15$, where E is the instantaneous laser electric field, m_e is the mass of an electron, and ω_0 is the laser frequency. The laser was focused onto the edge of a supersonic helium gas jet target that was produced using a 2-mm-diam nozzle. The gas jet backing pressure was varied to give plasma electron densities of up to 5×10^{19} cm⁻³. Analysis of the wavelength-shifted laser light scattered by forward Raman scattering instability provided a simultaneous measurement of the plasma electron density during the interaction.

The main diagnostic of the interaction was a temporally independent probe beam that passed through the interaction region in a direction orthogonal to the main high-intensity beam [Fig. 1(a)]. The probe-beam pulse was derived from the compressed main beam and frequency doubled to 527 nm using a KDP crystal. The accuracy of

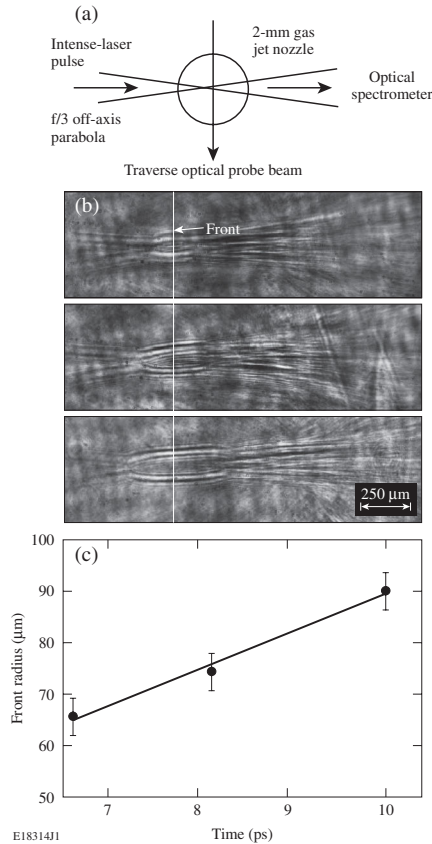


FIG. 1. (a) Experimental setup. (b) Front images in helium plasma interactions with $n_e = 1.6 \times 10^{19} \text{ cm}^{-3}$ and 350-TW, 1-ps-duration laser pulses. The white line indicates the focal plane of the laser. The laser propagates left to right. (c) Temporal evolution of the front radius.

the probe-beam timing with respect to the main interaction beam was comparable to the pulse duration. A lens magnified the interaction by $10\times$ and imaged it onto a 16-bit charge-coupled device (CCD) to form a shadowgraphy diagnostic channel.

Figure 1(b) shows three shadowgrams of the front that forms in helium plasma interactions with $n_e = 1.6 \times 10^{19} \text{ cm}^{-3}$ using 350-TW, 1-ps-duration laser pulses. The images were taken at $t = t_0 + 7 \text{ ps}$, $t = t_0 + 8 \text{ ps}$, and $t = t_0 + 10 \text{ ps}$, where t_0 is the arrival time of the main laser pulse at the edge of the gas jet. The white line indicates the focal plane of the laser. The images show the formation and evolution of a cylindrically symmetric front in the region of the laser focal plane. The front extends four to five vacuum Rayleigh lengths prior to the defocusing and filamenting of the laser pulse. This is indicative of the presence of relativistic self-focusing. The front radius as a function of time is plotted in Fig. 1(c). This measurement was made along the radial axis defined by the position of the laser vacuum focus. The data give an expansion velocity of $(7.9 \pm 1.8) \times 10^8 \text{ cm/s}$. The front maintained an approximately uniform front thickness over this 10-ps period of around $(50 \pm 10) \mu\text{m}$.

Figure 2(a) shows five shadowgrams of the front that forms in helium plasma interactions with $n_e = 2.0 \times 10^{19} \text{ cm}^{-3}$ using 200-TW, 1-ps-duration laser pulses. The images were taken 30, 70, 153, 225, and 231 ps after time $t = t_0$. The white line indicates the focal plane of the laser. The images show the formation and evolution of a cylindrically symmetric front that extends for several hundred microns prior to the laser defocusing and filamenting. In the first 70 ps, the front propagates at $(8.3 \pm 2.5) \times 10^7 \text{ cm/s}$. By 231 ps the front has traveled into the surrounding ambient gas and has reduced in velocity to $(1.1 \pm 1.0) \times 10^7 \text{ cm/s}$. The front radius as a function of time is plotted in Fig. 2(b). This measurement was made along the radial axis defined by the position of the laser vacuum focus. The front thickness along the same line is plotted in Fig. 2(c) and is observed to reduce in thickness.

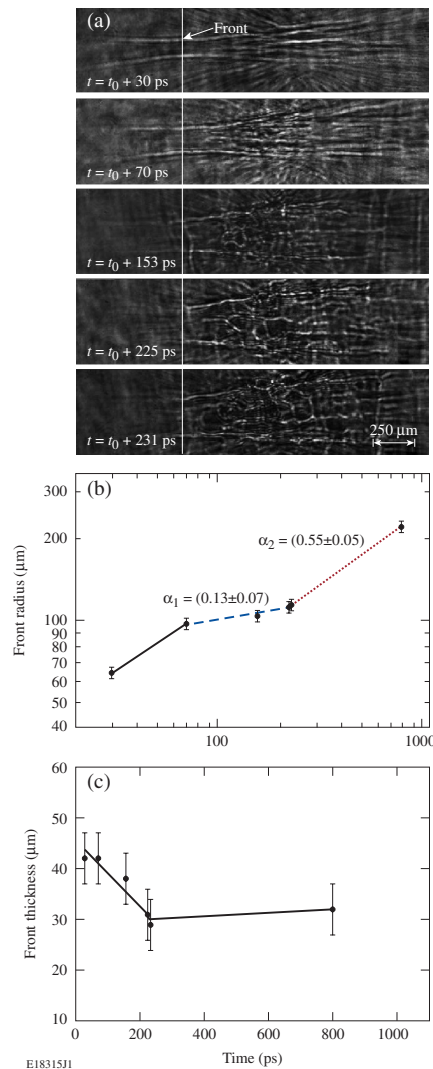


FIG. 2 (color online). (a) Front images in helium plasma interactions with $n_e = 2.0 \times 10^{19} \text{ cm}^{-3}$ using 200-TW, 1-ps-duration laser pulses. The white line indicates the focal plane of the laser. The laser propagates left to right. (b) Temporal evolution of the front radius and (c) front thickness along the radial axis defined by the laser focal plane.

The trajectory data indicate three stages in the front evolution. In the earliest stage, the system is dominated by a high-velocity, nonlocal electron heat wave [9]. In time, the data are described by a power law with exponent $\alpha_1 = (0.13 \pm 0.07)$. This transition is consistent with the electron mean free path becoming comparable to the temperature-gradient scale length across the propagating front and the formation of a thermal heat wave ($\alpha = 1/7$ in 2-D cylindrical geometry). After several hundreds of picoseconds, the shock front catches up with the electron thermal front, forming a blast wave [10–12]. The data support this transition and the power-law exponent becomes $\alpha_2 = (0.55 \pm 0.05)$, consistent with a nonradiative blast front.

The expanding front is observed to develop thin-shell instability [see Fig. 3(a)]. The instability developed following an earlier phase (Figs. 1 and 2) in which the front appears to be smooth. This is unlike any previous instability generated in a laser-generated blast wave since in helium plasmas, radiation effects are not expected to play an important role. Indeed, the thin shell perturbations have grown without the front fragmenting or breaking up. The front maintains an approximately uniform thickness across its transverse extent, while the instability has a wavelength and amplitude with a similar spatial scale as the front thickness itself. This instability has grown from noise following the front reducing in thickness, and by $t = t_0 + (800 \pm 200)$ ps, the unstable modes have been damped. The front thickness has stopped reducing in extent and remains approximately constant by this time [Fig. 3(b)].

The blast-front evolution is determined by collisionless electrostatic shock formation and the onset of collisional interactions as the shock wave enters the surrounding unionized gas. The ultrahigh-velocity collisionless shock is achieved by the transient, large-amplitude electric fields generated by charge separation caused by the ponderomo-

tive pressure of a relativistically self-focusing laser pulse [13,14]. The shock front thus generated was observed to reduce in thickness and subsequently develop significant corrugation instability. This occurred on a time scale consistent with a transition in the ion dynamics from a period of quasineutral collisionless expansion to collisional interaction of the ions with the neutral gas and the consequent ionization of the helium atoms. Indeed if an estimate is made of the energy contained in the hot ions generated initially in the shock wave, i.e., a radius of 5- μm diameter with an average energy of 500 keV [6], the system contains sufficient energy to ionize helium (ionization potentials 24 and 54 eV) over a radius of a few hundred microns before the shock is significantly depleted. This distance is consistent with the 100 μm shock front radius in our experiments [Fig. 2(b)] in which the shock is observed to slow down and become thinner, signaling the transition from collisionless expansion to collision dominated behavior.

To understand the electrostatic shock-launching mechanism, a 2D particle-in-cell simulation of the interaction was performed (Fig. 4) [15]. In the simulation electrons and ions started to lag the main front and form the emergent backfill of the previously formed cavity. Over the simulation, the electric field across the front reduced in accordance with energy dissipation and the loss of electrons and ions to the quasineutral, forward-propagating front, and the quasineutral plasma that lags the principal front. The ultrahigh shock velocity generated in these simulations was similar to that observed in our experiments at early times. These simulations are also in qualitative agreement with work [13,14] at lower intensities.

Concerning the instability at later times, Dyakov and Kontorovich (DK) [16] have previously investigated perturbation instability imposed on the surface of a shock wave. They found that perturbation growth was linked to the emission of acoustic waves from the front and identified the conditions under which these perturbations grew. The criteria for corrugation instability growth were linked to the Hugoniot-curve shape. In particular, the DK instability is present if the Hugoniot slope lies below a threshold value, i.e., $h_c = [1 - M_2^2(1 + V_1/V_2)]/[1 - M_2^2(1 - V_1/V_2)]$ where M is the Mach number of the flow, and $h = j^2(dV/dp)_H$, where $j^2 = (p_2 - p_1)/(V_1 - V_2)$ is the square of the mass flow density (1 and 2 are the upstream and downstream fluids with respect to the shock front). The derivative in the definition of h is taken along the Hugoniot curve.

For an ideal gas it is not possible to satisfy this condition; however, for complex Hugoniot shapes such as those associated with ionizing shocks, the threshold can be met. This has been demonstrated theoretically and in simulations [17,18] and has also been observed in low-Mach-number ionizing shocks driven by shock tubes [19]. The original need for modification of the standard DK criteria arose as the application of the latter failed to explain the

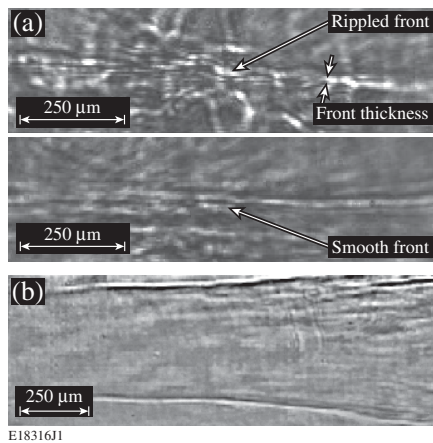


FIG. 3. (a) Images of the rippled front structure at $t = t_0 + 233$ ps and the smooth front structure at $t = t_0 + 70$ ps with $n_e = 2.0 \times 10^{19} \text{ cm}^{-3}$ and 200-TW, 1-ps-duration laser pulses. (b) Front image with $n_e = 2.0 \times 10^{19} \text{ cm}^{-3}$ and 200-TW, 1-ps-duration laser pulses taken at $t = t_0 + (800 \pm 200)$ ps.

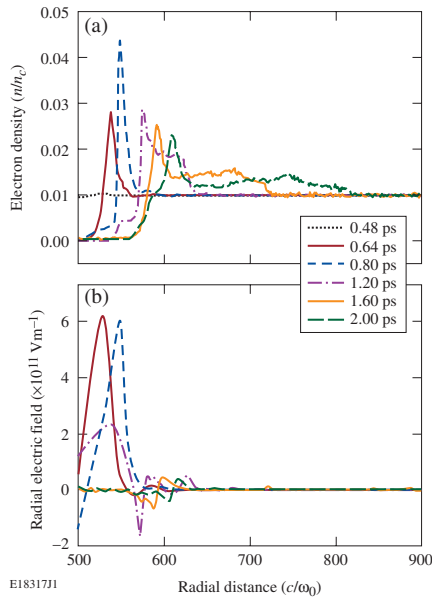


FIG. 4 (color online). OSIRIS code results for different time steps showing (a) the evolution of electron density and (b) the magnitude of the radial electric field.

accumulating observations of irregular behavior behind strong shocks. The conditions for this instability are also likely appropriate for the highly nonlinear ionizing shocks generated in our experiments. Indeed the thermal nonequilibrium between the electrons that are produced by the electron-atom ionization process in ultrahigh-intensity, laser-driven plasmas and the remaining atoms and ions can play a decisive role in the onset of DK instability. In addition, DK instability has been shown to eventually decay away—in agreement with our experimental observations [18] (Fig. 3). Such instabilities will be important in highly nonlinear situations in which there is a significant temperature difference between the plasma electrons and ions as found in the period up to blast-front formation. It has been shown that a single ionization process can provide the main mechanism for DK instability and excitations of the electronic energy levels of atoms or ions result only in a slight modification of the instability threshold [18]. Future quantitative studies of the experimental DK growth rate may now be realized based on the work presented here to study the detailed development of the instability.

In conclusion, optical probing measurements have been presented of ultrastrong collisionless shocks within underdense plasmas irradiated at intensities $>10^{20}$ W/cm². These are the first observations of such ultrahigh-velocity collisionless shocks in the laboratory that approach the relativistic regime. An important aspect of these interactions is instability formation as the shocks propagate into a surrounding gas and form blast waves. These results are potentially interesting for the laboratory study of a unique class of shocks relevant to the understanding of some important astrophysical situations.

The authors acknowledge the assistance of the staff of the Central Laser Facility of the Rutherford Appleton Laboratory and the support of the UK Engineering and Physical Sciences Research Council (EPSRC). We gratefully acknowledge the OSIRIS Consortium, which consists of UCLA/IST (Portugal)/USC for the use of OSIRIS. K. K. acknowledges useful discussions with Professor R. P. Drake.

*Present address: LLE and FSC, University of Rochester, Rochester NY, USA.

†Present address: Center for Ultrafast Optical Science, University of Michigan, Ann Arbor, MI, USA.

‡Present address: Institute for Optics and Quantum Electronics, Jena, Germany.

- [1] C. F. McKee and B. T. Draine, *Science* **252**, 397 (1991).
- [2] J. P. Ostriker and C. F. McKee, *Rev. Mod. Phys.* **60**, 1 (1988).
- [3] J. Grun *et al.*, *Phys. Rev. Lett.* **66**, 2738 (1991).
- [4] M. J. Edwards *et al.*, *Phys. Rev. Lett.* **87**, 085004 (2001); A. S. Moore, D. R. Symes, and R. A. Smith, *Phys. Plasmas* **12**, 052707 (2005); A. D. Edens *et al.*, *Phys. Rev. Lett.* **95**, 244503 (2005); A. B. Reighard *et al.*, *Phys. Plasmas* **13**, 082901 (2006); S. Bouquet *et al.*, *Phys. Rev. Lett.* **92**, 225001 (2004).
- [5] T. Ditmire and A. D. Edens, *Laser Photon. Rev.* **2**, 400 (2008).
- [6] M. S. Wei *et al.*, *Phys. Rev. Lett.* **93**, 155003 (2004).
- [7] T. J. Gaetz *et al.*, *Astrophys. J.* **534**, L47 (2000).
- [8] P. A. Norreys, K. M. Krushelnick, and M. Zepf, *Plasma Phys. Controlled Fusion* **46**, B13 (2004).
- [9] T. Ditmire *et al.*, *Phys. Rev. Lett.* **80**, 720 (1998).
- [10] A. S. Moore, D. R. Symes, and R. A. Smith, *Phys. Plasmas* **12**, 052707 (2005).
- [11] A. S. Moore *et al.*, *Astrophys. Space Sci.* **307**, 139 (2007).
- [12] G. Taylor, *Proc. R. Soc. A* **201**, 159 (1950); L. I. Sedov, *Similarity and Dimensional Methods in Mechanics* (Academic, New York, 1959).
- [13] K. Krushelnick *et al.*, *Phys. Rev. Lett.* **83**, 737 (1999).
- [14] G. S. Sarkisov *et al.*, *Phys. Rev. E* **59**, 7042 (1999).
- [15] R. G. Hemker *et al.*, in *Proceedings of the 1999 Particle Accelerator Conference*, edited by A. Luccio and W. MacKay (IEEE, New York, 1999); R. A. Fonseca *et al.*, in *Computational Science ICCS 2002*, edited by P. M. A. Sloot *et al.*, Lecture Notes in Computer Science Vol. 2331 (Springer, Berlin, 2002), p. 342.
- [16] S. P. Diakov, *J. Exp. Theor. Phys.* **27**, 288 (1954); V. M. Kontorovich, *J. Exp. Theor. Phys.* **33**, 1525 (1957); V. M. Kontorovich, *Akust. Zh.* **5**, 314 (1959).
- [17] M. Mond, I. Tutkevich, and E. Toffin, *Phys. Rev. E* **56**, 5968 (1997).
- [18] J. W. Bates and D. C. Montgomery, *Phys. Fluids* **11**, 462 (1999); J. W. Bates and D. C. Montgomery, *Phys. Rev. Lett.* **84**, 1180 (2000); J. W. Bates, *Shock Waves* **12**, 31 (2002).
- [19] R. W. Griffiths, R. J. Sandeman, and H. G. Hornung, *J. Phys. D* **9**, 1681 (1976).